STATIC AND FORCED OSCILLATION TESTS ON A GENERIC COMBAT AIRCRAFT MODEL

C.O. O'Leary, B. Weir and J.M. Walker
Defence Research Agency, Bedford, United Kingdom

Abstract

Static and small-amplitude oscillatory tests were made on a generic combat aircraft model as part of an AGARD-FDP Working Group activity. The objective of the Group was to further the understanding of manoeuvring aerodynamics at high angle of attack through a cooperative programme of experimental and analytical work. This paper reports on the effects of forebody strakes and transition fixing, frequency of oscillation and the presence of leading-edge root extensions on the static forces and aerodynamic derivatives.

Introduction

Background

A Working Group (WG 16) of the Fluid Dynamics Panel of AGARD has recently completed a "Cooperative programme on dynamic wind-tunnel experiments for manoeuvring aircraft". The objective of the Working Group was to further our understanding of manoeuvring aerodynamics at high angle-of-attack. A generic combat aircraft model was designed, manufactured and tested on various continuous rotation and forced oscillation rigs in Europe and North America. These cooperative experiments on the same configuration were the focus of a systematic study of various aspects of dynamic testing and manoeuvring aerodynamics. Included in the study were the physics of rotary and oscillatory flows, effects of tunnel and model support interference, Reynolds number, forebody transition fixing, model configuration and forebody nose strakes. The general aim was to cooperatively study these topics so that manoeuvring, departure and spinning characteristics of future combat aircraft could be predicted more accurately. The present paper describes results from static and small amplitude forced oscillation tests using the DRA Inexorable Drive Rig (IDR).

Forced oscillation tests

Results from forced oscillation tests are valuable in assessing the basic stability characteristics of an aircraft configuration and have applications in the prediction of flight manoeuvres and in setting-up flight simulations. The IDR, developed at DRA Bedford[1], can oscillate models in 5 degrees-of-freedom: pitch, plunge, yaw, sway and roll. Measurements are made of the dynamic derivatives, e.g. C_{nr}, the yaw damping, as well as the so-called static derivatives, e.g. $C_{n\beta}$, the directional stability. These data are measured dynamically, and consequently would be more relevant to manoeuvring flight than the displacement derivatives obtained from static wind-tunnel tests.

Description of model

General description

The configuration selected for the WG 16 cooperative programme is shown in figure 1. It is based on the NASA Langley/Eidetics generic combat aircraft model. The body is cylindrical with a tangent-ogive nose of relatively high fineness ratio (length/diameter = 4). The wings, tail surfaces and leading edge root extensions (LEX) are of flat-plate section with chamfered leading and trailing edges and tips. Wing leading edges are swept at 45°. Both models were manufactured to allow configuration build-up tests with body alone, body-wing, body-wing-LEX and body-wing-LEX-horizontal/vertical tail surfaces. During initial tests[1] the models were fitted with forebody nose strakes and longitudinal strips for transition fixing as described below and shown in figure 2. Three models were manufactured for testing in Europe and North America and designated WG16A, WG16CA and WG16B. The WG16A and WG16CA models are nominally identical but WG16B is smaller, at 0.73 of the scale of the other two models. The DRA rotary tests[1] were made with WG16B but the static and oscillatory tests described here were made with WG16A. The body of WG16A was turned from aluminium alloy in six sections, 1.5 mm thick, with integral formers for local stiffness and strength, especially where wings and tail surfaces are attached. The wings and tail surfaces are made of aluminium alloy/honeycomb sandwich material which consists of 1 mm thick aluminium plates bonded on to a honeycomb core. The edges of the surfaces are made of glass-epoxy composite and are 40° included angle, except the wing tips which are 60°. Wing and vertical tail root fittings are aluminium alloy but the adjustable horizontal tail fitting is steel. The LEX is made of plastic.The model weighs approximately 6.5 kg; In this paper the various components of the model are abbreviated as follows:

B = body; W = wings; L = leading edge root extension (LEX); H = horizontal tail; V = vertical tail; S = forebody nose strakes; T= transition fixing (grit strips)

Nose strakes and transition fixing

It is well known that the flow on high-fineness ratio forebodies, such as the one on the WG16 model, are characterized by asymmetric vortex flow regimes at angles-of-attack above a certain onset value. For values of angles-of-attack above onset of asymmetry the flow is highly dependent on model micro-asymmetries and random disturbances and also on boundary layer transition positions and test Reynolds number. Although the high sensitivity of the test configuration may be desirable for highlighting any spurious interference effect, the random character of asymmetric vortex flow may also make the interpretation and comparison of test results an impossible task. For this reason it was decided that the test should not only consider the basic clean forebody, but also an alternate configuration where the flow was manipulated in a way to make it more predictable and repeatable. This could be obtained by avoiding random effects due to uncertain boundary layer transition and by fixing the separation points on the apex of the forebody by using nose strakes. Position and size of such devices were selected during initial tests of model WG16B at DRA[1]. Details are shown in figure 2. Roughness bands were applied at radial locations ±40° from the bottom centre line running from the tip of the nose to the LEX apex. These devices consisted of "grit" 0.2 to 0.3 mm in height. Forebody strakes were fitted at radial positions of ±105°, one fuselage diameter in length and 0.1 diameters in height above the forebody surface at the trailing edge. The strakes were attached perpendicular to the forebody surface.

Description of apparatus

Mechanical components

For static tests the model was sting-mounted on a conventional six-component strain gauge balance as shown in figure 3. Angle-of-attack was varied by means of the twin-leadscrew arrangement and angle-of-sideslip by rotation of the floor and ceiling turntables to which the rig is fixed. The rear sting crank angle was variable to allow tests up to 50° angle-of-attack.

The main component of the IDR, shown in figure 4, is a model support sting which can be oscillated in five degrees-of-freedom, i.e. pitch, plunge (heave), yaw, sway (sideslip) and roll. The rig is shown configured for plunge (figure 4a) and pitch (figure 4b) oscillation: for sway and yaw the sting and swinging arm assembly are fitted at 90° to that shown. For the roll mode the sting is axially driven by the motor shaft. Forces acting on the model are measured by a strain gauge balance which is integral to the sting.

For all modes except the roll mode the flared downstream end of the sting is mounted on the swinging arm assembly which converts a rotational shaft drive on the wind-tunnel axis to oscillatory harmonic motion using a 'scotch yoke' slider-in-slot mechanism. The sleeve mounting for the swinging arms fits over the shaft housing and the base plate is bolted to the support structure in either of the two positions. Amplitude of the motion is varied by adjusting the throw of the slider within a limit of ±50 mm. The slot is aligned horizontally for pitch and plunge motion and vertically for yaw and sway motion. Change of alignment is accomplished by rotating the assembly through 90°. For translational motion, i.e. plunge and sway, the swinging arms are parallel. For pitch and yaw motion the rear stationary pivots of the swinging arms are moved further apart as shown in figure 4b. The centre of oscillation coincides with the balance axis. Frequency of oscillation is dependent on shaft speed which is controlled by a servo valve.

For the roll mode the shaft is rigidly connected to the sting and an oscillatory signal to the servo valve gives the required oscillatory motion about the sting axis.

A hydraulic power pack, situated outside the wind-tunnel working section supplies the motor with fluid at 1500 psi pressure via a rigid pipe and swivel joint linkage not shown in figure 4. The drive mechanism is mounted on a carriage which is traversed along the twin support quadrants to vary angle-of-attack up to a limit of 42°. For all modes, except roll, model motion is measured with an accelerometer in the model, linear for plunge and sway tests and angular for pitch and yaw tests. These accelerometer signals are also used to cancel inertial loadings on the strain gauge balance. The sensitive axes of the accelerometers are re-aligned in the appropriate direction for each type of test. For the rolling mode, motion is measured with a displacement transducer (LVDT).

Data acquisition system

For static tests the strain gauge balance signals were amplified, filtered and digitised by means of dedicated panel meters and the resulting signals processed by the tunnel computer to display aerodynamic coefficients. The data were further corrected for tunnel constraint, blockage, etc during post-test processing.

The data acquisition system for IDR tests consists of a signal processing unit, A-to-D converter and Fourier Transform software on a Masscomp computer. Strain gauge balance signals and the accelerometer or LVDT signal are amplified and filtered using phase and gain matched 20Hz filters. In addition, phase lags are introduced in the strain gauge signals so as to match the accelerometer or LVDT

signal to better than 0.2 deg. over the frequency range of the tests. Interactions are eliminated within a signal mixing unit. After conversion to digital form the in-phase and in-quadrature components of the signals are determined using a discrete Fourier Transform and the components normalised with respect to the reference accelerometer or LVDT signal. After testing, the data is down-loaded onto a PC for post-test data reduction and analysis.

Tests made

Static tests

The objective of these tests was to measure the effect of the forebody transition fixing and nose strakes on the variation of forces and moments with angle-of-attack. Tests were made on the body alone and on the complete configuration at a wind speed of 30 m/s in the 13ft x 9ft atmospheric wind tunnel. Only results for the complete configuration are given in this paper. The test angle-of-attack range was 0° to 48° at $\beta = 0°$.

Forced oscillation tests

These tests were made on the 5 degree-of-freedom Inexorable Drive Rig in the 13ft x 9ft wind tunnel. Test speed was again 30 m/s. The angle-of-attack range was 0° to 42° and all tests were made at $\beta = 0°$.

The objectives were to determine the effects of:
a. forebody transition fixing and nose strakes,
b. frequency of oscillation and
c. the presence of the LEX
on the variation of the longitudinal and lateral aerodynamic derivatives with angle-of-attack.

Results and discussion

All coefficients and derivatives are referred to body axes and are defined in the List of Symbols.

Effect of nose strakes and grit strips

The combined effect of nose strakes and grit strips on C_N, C_m, C_Y and C_n is shown in figure 5. Normal force and nose-up pitching moment are reduced at high angles-of-attack when the model was tested with nose strakes and grit strips. For $\alpha > 35°$, the nose strakes and grit strips reduce the large sideforces and yawing moments to virtually zero, indicating that these devices are effective in suppressing the formation of asymmetric forebody vortices at high angle-of-attack. Results from ONERA-IMFL tests on the same model in configuration BWLHVST are in good agreement with DRA measurements. Results from pitch, plunge and yaw tests are shown in figure 6. The derivative $(C_{Nq} + C_{N\dot{\alpha}})$ is measured in the pitching mode as an in-quadrature component and the component due to $\dot{\alpha}$, $C_{N\dot{\alpha}}$ is measured in the plunging mode as an in-phase component. The variation of $(C_{Nq} + C_{N\dot{\alpha}})$ and $C_{N\dot{\alpha}}$ is similar with and without strakes and grit strips except that the large changes in magnitude in the region of $\alpha = 20°$ occur at a slightly lower angle-of-attack with strakes and grit strips. It is apparent that the large changes are due to the variation in the $\dot{\alpha}$ component.

The combined damping-in-yaw derivative $(C_{nr} - C_{n\dot{\beta}} \cos)$ measured in the yawing mode (figure 6) shows that for $\alpha < 15°$ there is little difference with and without grit and strakes. In the range $20° < \alpha < 33°$ the derivative is positive (negative damping) for tests with strakes and grit strips, whereas without these devices there is damping throughout the test angle-of-attack range. From the measurement of $C_{n\dot{\beta}}$ in the swaying mode, shown later in figure 9, this positive trend is mostly due to the contribution from the $C_{n\dot{\beta}}$ component. It is therefore likely that the differences are due to the effect of the nose strakes and grit strips on the behaviour of the forebody vortices for varying $\dot{\beta}$.

The results show that the nose strakes and longitudinal transition fixing strips have an important effect on the static and dynamic characteristics of the model at high angle-of-attack. Sideforces at $\beta = 0°$ are suppressed at high angle-of-attack but the forebody devices have a de-stabilising effect on the damping-in-yaw derivative. Thus, on configurations with high fineness ratio forebodies, the presence of cross-flow control devices may affect both dynamic and static characteristics.

Effect of frequency

Results from pitch and plunge tests at two frequencies, $\Omega_t = 0.08$ and 0.16, are shown in figure 7. Most of the effect of frequency on $(C_{mq} + C_{m\dot{\alpha}})$ and $C_{m\dot{\alpha}}$ is likely to originate from a downwash lag effect at the tail but, taking account of the scatter shown in repeat measurements of $C_{m\dot{\alpha}}$ at high α, it appears that the effect on pitching moment is small. However, differences in $(C_{Nq} + C_{N\dot{\alpha}})$ for $\alpha > 25°$ are appreciable and mostly due to the effect of frequency on the $C_{N\dot{\alpha}}$ component as indicated by the plunging mode measurement of this derivative. It is likely that with varying $\dot{\alpha}$, frequency has an effect on the chordwise lag in normal force on the forebody, LEX and wings, which is the main contributor to $C_{N\dot{\alpha}}$.

Measurements of the lateral/directional "stiffness" derivatives $C_{n\beta}$, $C_{Y\beta}$ and $C_{l\beta}$ from static tests are compared with results from oscillatory tests at two frequencies in figure 8. Derivatives from static tests were determined by measuring the gradient of C_n, C_Y and C_l vs

β for $\beta = 0°, \pm 5°$. The dynamic data were obtained from in-phase measurement in the yawing mode, where the amplitude was $\pm 2°$. The gradients of the static forces over $\beta = \pm 5°$ are therefore an approximate equivalent to the oscillatory derivatives. At low angle-of-attack, the static measurement of $C_{Y\beta}$ is more negative than the dynamic data and $C_{n\beta}$ is positive, whereas the dynamic $C_{n\beta}$ shows neutral stability. At high angle-of-attack, however, the static $C_{n\beta}$ is more negative. Differences in $C_{n\beta}$ and $C_{Y\beta}$ due to reduced frequency change from 0.144 to 0.288 are small.

There is also a difference between the static and dynamic measurements of $C_{l\beta}$. Statically, $C_{l\beta}$ increases in magnitude, progressively, with angle-of-attack up to $\alpha = 24°$, after which there is a gradual reduction; whereas results from oscillatory tests at both frequencies show large changes in magnitude for $13° < \alpha < 22°$ and a greater positive (unstable) trend at higher angles-of-attack. Similar differences between static and dynamic $C_{l\beta}$ were noted on another model[2].

These differences between static and dynamic measurements of lateral derivatives due to angular displacement β show that care must be taken when these data are used to predict flight characteristics or when setting up flight simulations. For representation of manoeuvring flight, data from oscillatory tests may be more appropriate.

Effect of LEX

Results from pitch, plunge, yaw and sway tests with and without the LEX are shown in figure 9 for the complete configuration with forebody strakes and grit strips.

Effects of the LEX on the normal force derivatives $(C_{Nq} + C_{N\dot{\alpha}})$ and $C_{N\dot{\alpha}}$ are pronounced. In the angle-of-attack range $6° < \alpha < 34°$ both derivatives are more positive with the LEX off except where there is a 'spike' in the LEX-on characteristic at $\alpha \approx 20°$. It is apparent that for $\alpha > 5°$ it is the $\dot{\alpha}$ component of $(C_{Nq} + C_{N\dot{\alpha}})$ which predominates and contributes most of the variation in the combined derivative. These results suggest that the LEX has a marked effect on the chordwise lag in normal force on the model. A discontinuity in the LEX-on characteristics at $\alpha \approx 20°$ may be due to LEX vortex breakdown or a LEX/wing vortex interaction effect.

Results from yaw and sway modes are also shown in figure 9. Differences in the yawing moment derivatives due to the LEX are most noticeable in the angle-of-attack range $20° < \alpha < 35°$ where the $\dot{\beta}$ component measured in the sway mode is the main contributor. The main contribution to $C_{n\dot{\beta}}$ is probably the lag of sidewash at the fin and the results suggest that the wake from the LEX modifies this sidewash lag.

Repeatability of test data

To check on repeatability of test data some test runs were repeated and an example of the results from two pitching mode tests (not consecutive) is shown in figure 10. In general, agreement between the two sets of data is good, including the 'spike' in the variation of $(C_{Nq} + C_{N\dot{\alpha}})$ at $\alpha \approx 20°$.

Conclusions

Tests

Static and 5 degree-of-freedom oscillatory wind-tunnel tests have been made on a generic combat aircraft model designated AGARD-FDP WG16A. The test objectives were to investigate the effects on static forces and aerodynamic derivatives of the following:

a) Forebody nose strakes and transition fixing
b) Frequency of oscillation
c)The presence of leading edge root extensions (LEX)

Effect of forebody nose strakes and transition fixing

On a model with a high fineness ratio forebody, nose strakes and cross-flow grit strips suppressed sideforces due to asymmetric forebody vortices which developed as angle-of-attack was increased at $\beta = 0°$. Even in the presence of the LEX the forebody devices had an effect on the static and dynamic characteristics. However, damping-in-yaw became negative at some angles-of-attack.

Effect of oscillation frequency

There were appreciable differences between static and dynamic measurements of the lateral/directional stiffness derivatives $C_{n\beta}$, $C_{Y\beta}$ and $C_{l\beta}$ which may have implications for prediction and simulation of manoeuvring flight.

Frequency effects were also apparent on derivatives due to $\dot{\alpha}$ and $\dot{\beta}$.

Effect of LEX

The presence of the LEX had a marked effect on derivatives due to $\dot{\alpha}$ and $\dot{\beta}$, i.e. $C_{N\dot{\alpha}}$, $C_{n\dot{\beta}}$. It is likely that the LEX modified the chordwise and spanwise flow lag effects which contributed to these derivatives.

General

The test results have furthered the understanding of

aerodynamic phenomena which have a bearing on the manoeuvring characteristics of combat aircraft .

References

1 O'Leary C.O., Weir B. and Walker J. M. *'Continuous rotation tests on a generic combat aircraft model in a low speed wind tunnel'*, DRA Tech Memo AERO/PROP 42 (1993)

2 O'Leary C.O., Weir B. and Walker J.M. *'A new rig for the measurement of rotary and translational derivatives'* ICAS-94-3.4.1 (1994)

List of symbols

AR	aspect ratio
b	wing span, m
c	aerodynamic mean chord, m
C_l	rolling moment / qSb
C_m	pitching moment / qSc
C_n	yawing moment / qSb
C_N	normal force / qS
C_Y	sideforce / qS
MRC	moment reference centre
p	rate of roll, rad/sec
q	dynamic pressure, N/m^2
q	rate of pitch, rad/sec
r	rate of yaw, rad/sec
S	wing area, m^2
V	wind speed
α	angle-of-attack, rad or deg
$\dot{\alpha}$	rate of change of angle of attack, rad/sec
β	angle-of-sideslip, rad or deg
$\dot{\beta}$	rate of change of angle of sideslip, rad/sec
ω	circular frequency, rad/sec
Ω_b	frequency parameter for yaw, sway and roll tests, $\omega b/2V$
Ω_c	frequency parameter for pitch and plunge tests, $\omega c/2V$

derivatives:

$C_{l\beta} = \partial C_l/\partial\beta$
$C_{m\alpha} = \partial C_m/\partial\alpha$
$C_{n\beta} = \partial C_n/\partial\beta$
$C_{N\alpha} = \partial C_N/\partial\alpha$
$C_{Y\beta} = \partial C_Y/\partial\beta$
$C_{l\dot{\beta}} = \partial C_l/\partial(\dot{\beta}b/2V)$
$C_{m\dot{\alpha}} = \partial C_m/\partial(\dot{\alpha}c/2V)$
$C_{n\dot{\beta}} = \partial C_n/\partial(\dot{\beta}b/2V)$
$C_{N\dot{\alpha}} = \partial C_N/\partial(\dot{\alpha}c/2V)$
$C_{lr} = \partial C_l/\partial(rb/2V)$
$C_{mq} = \partial C_m/\partial(qc/2V)$
$C_{nr} = \partial C_n/\partial(rb/2V)$
$C_{Nq} = \partial C_N/\partial(qc/2V)$

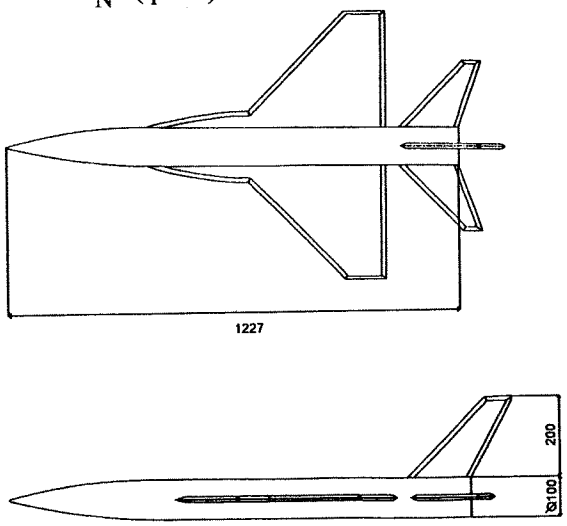

FIGURE 1 - General arrangement of generic combat aircraft model AGARD-FDP WG16A

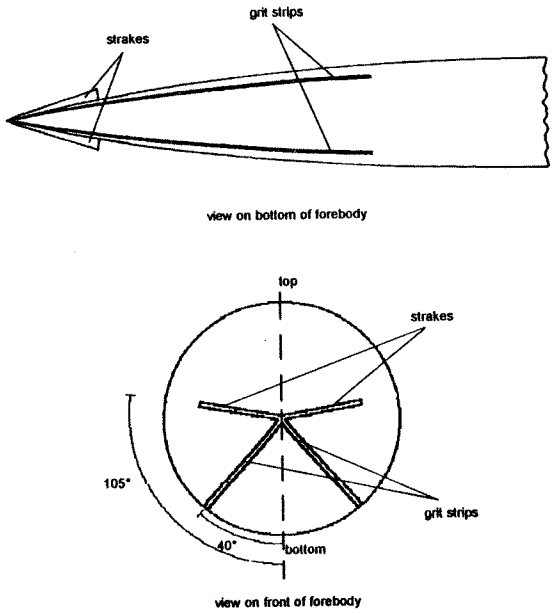

FIGURE 2 - General arrangement of forebody nose strakes and grit strips

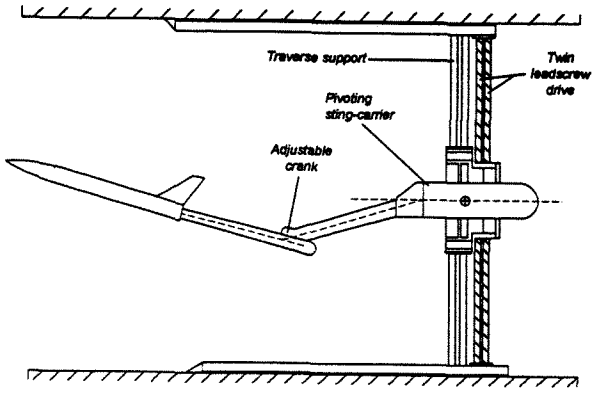

FIGURE 3 - Rig for static tests

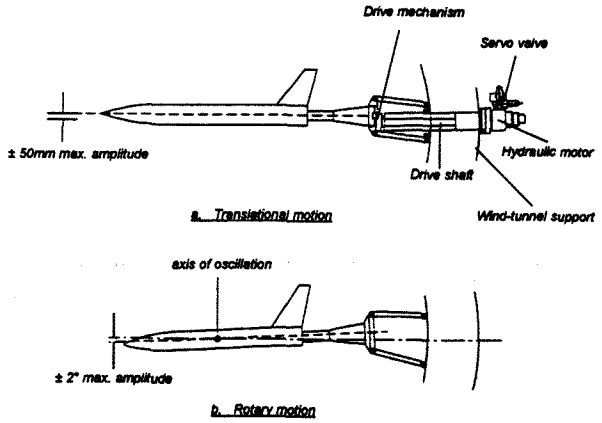

FIGURE 4 - Inexorable Drive Rig for oscillatory tests

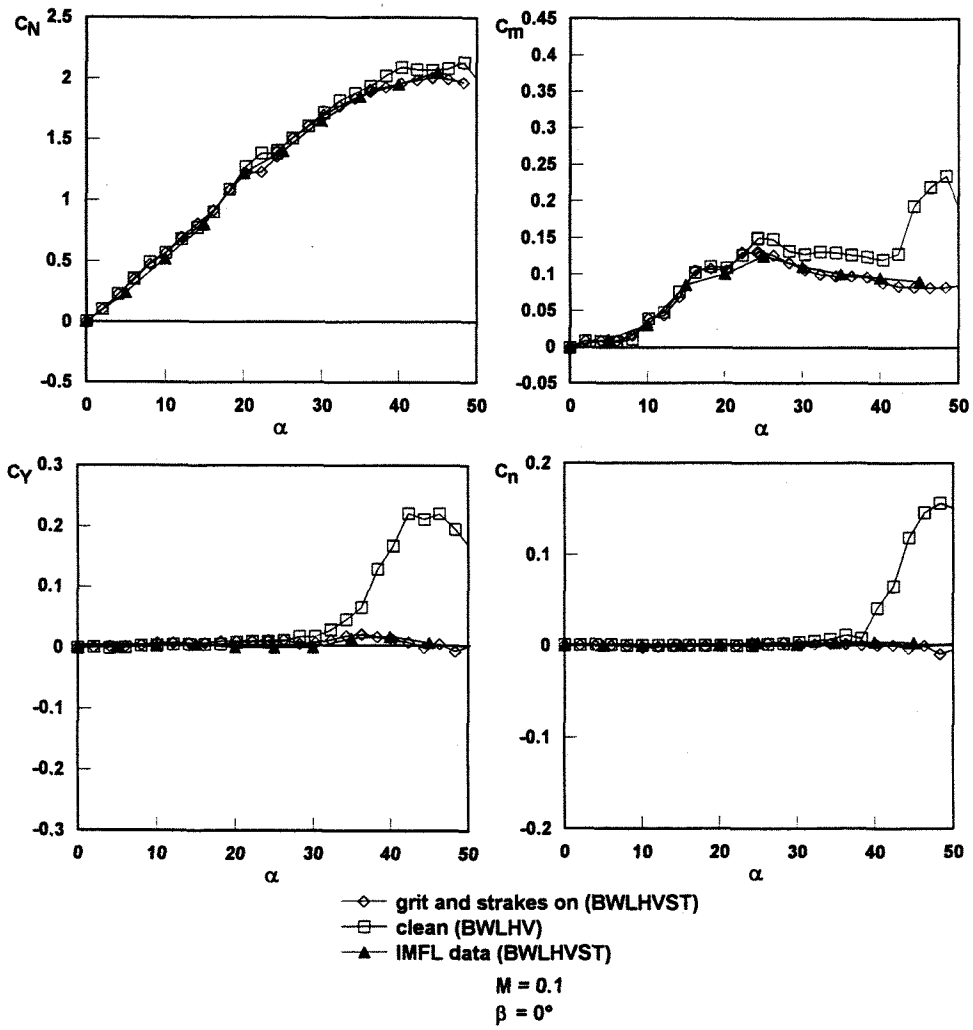

FIGURE 5 - Effect of forebody strakes and grit strips on static coefficients

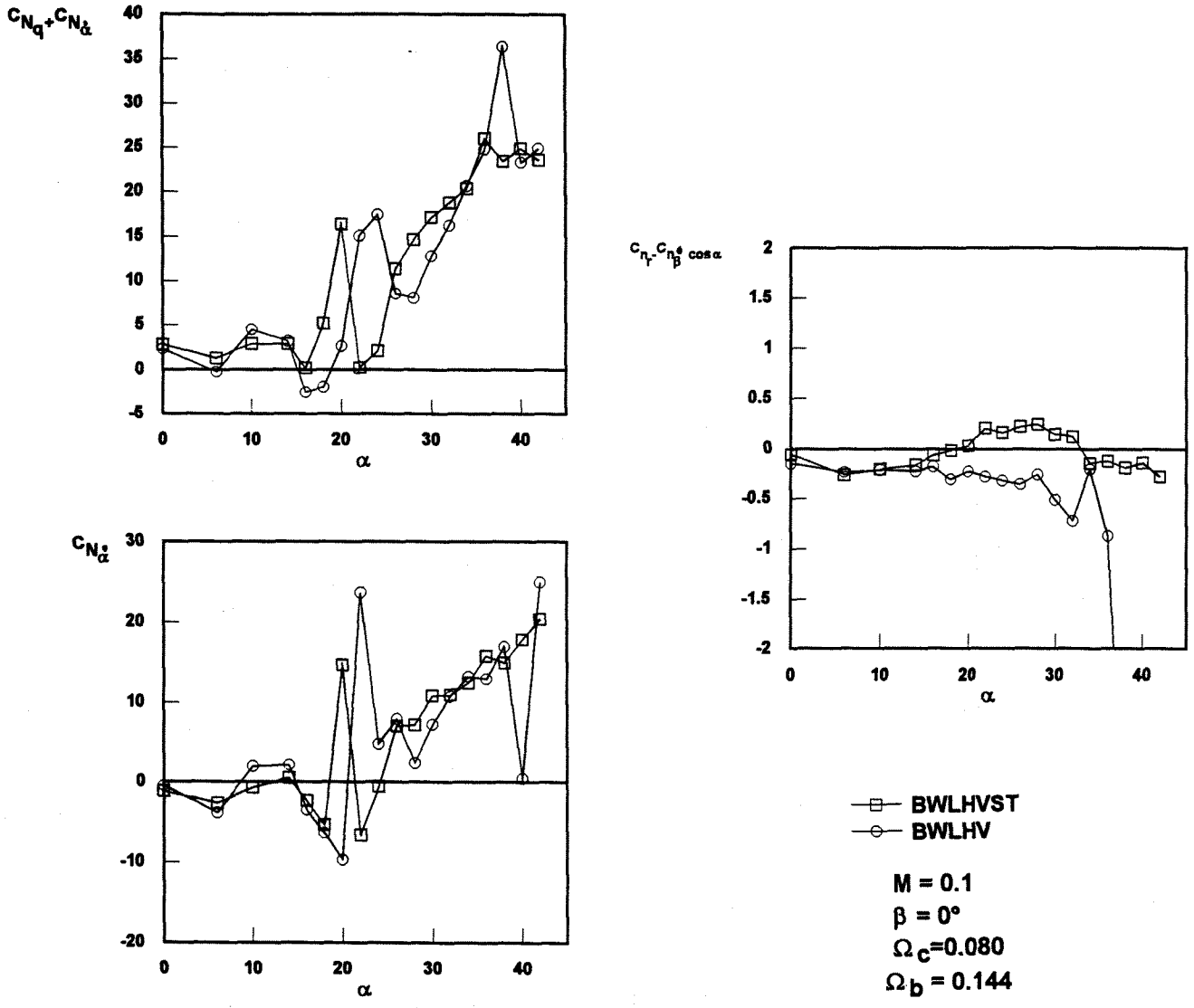

FIGURE 6 - Effect of forebody strakes and grit strips on dynamic derivatives

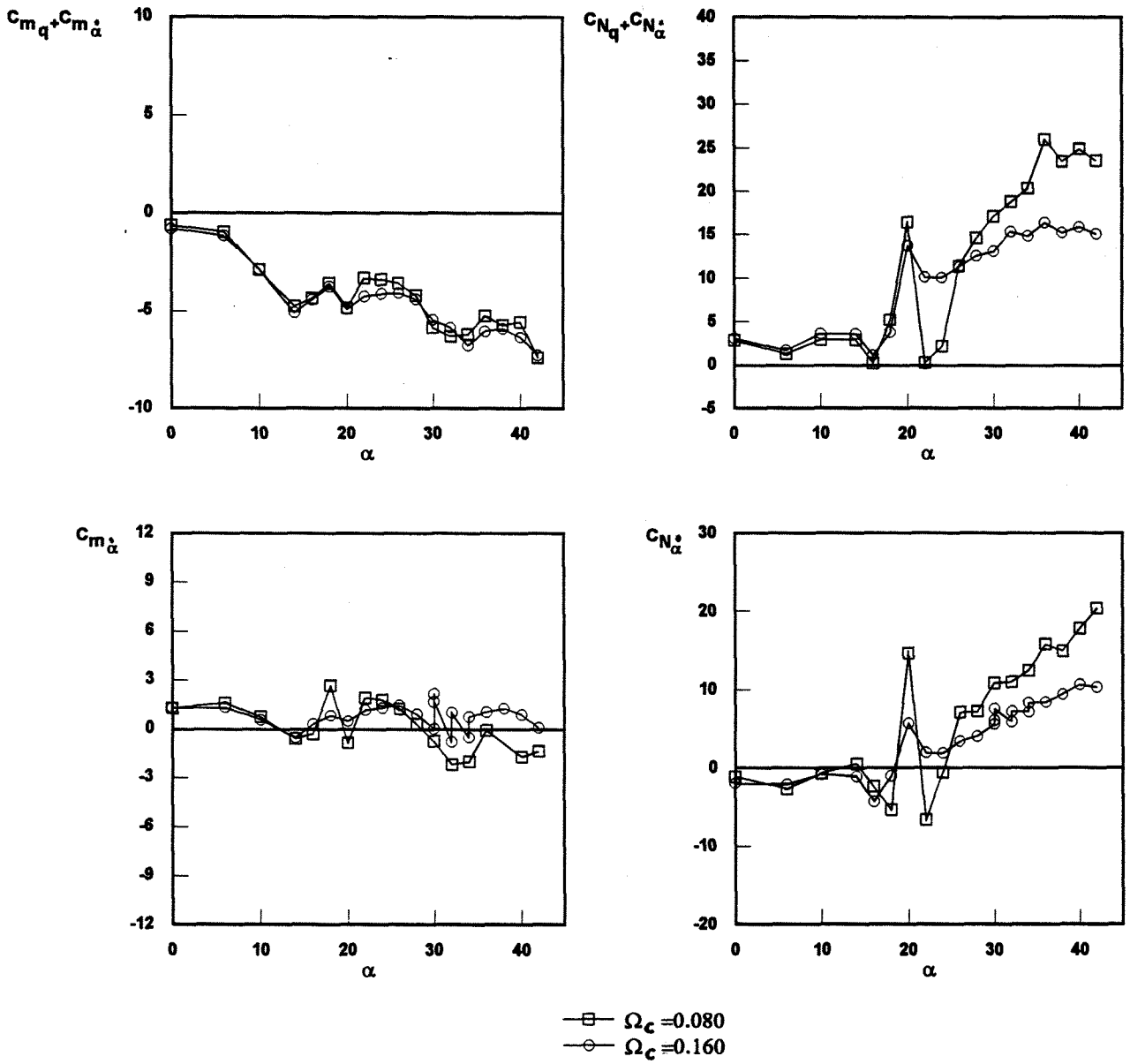

FIGURE 7 - Effect of frequency on derivatives from pitch and plunge modes

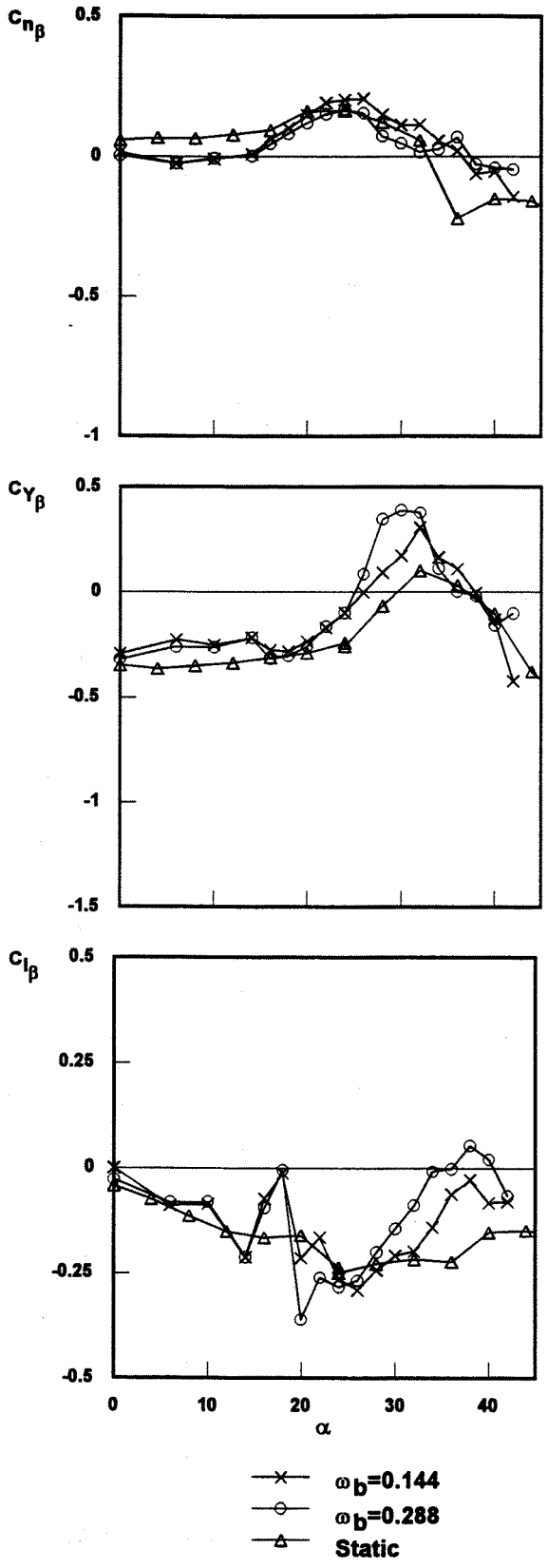

Configuration : BWLHVST

FIGURE 8 - Comparison of static and dynamic measurements of derivatives due to β

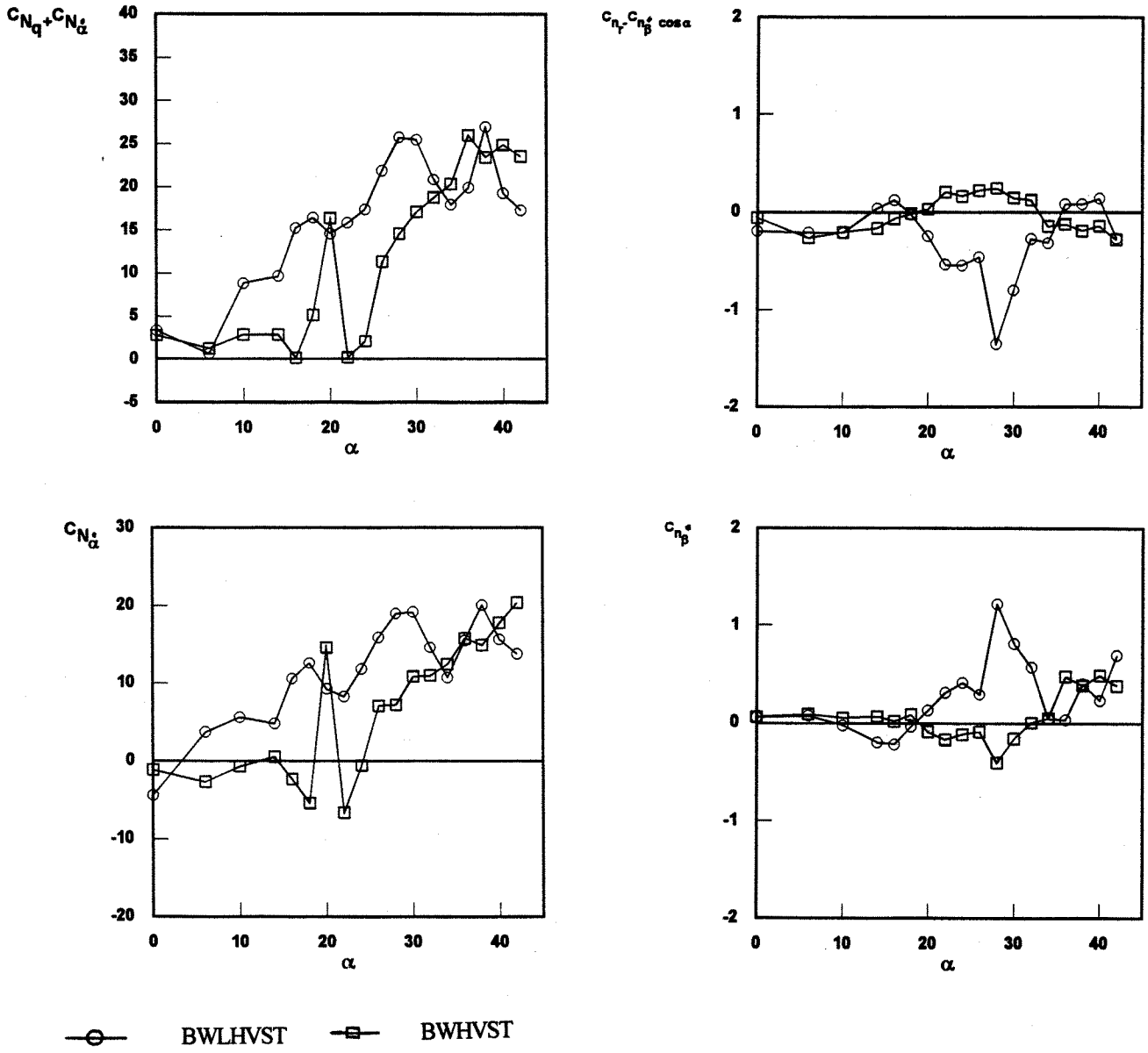

FIGURE 9 - Effect of LEX on dynamic derivatives

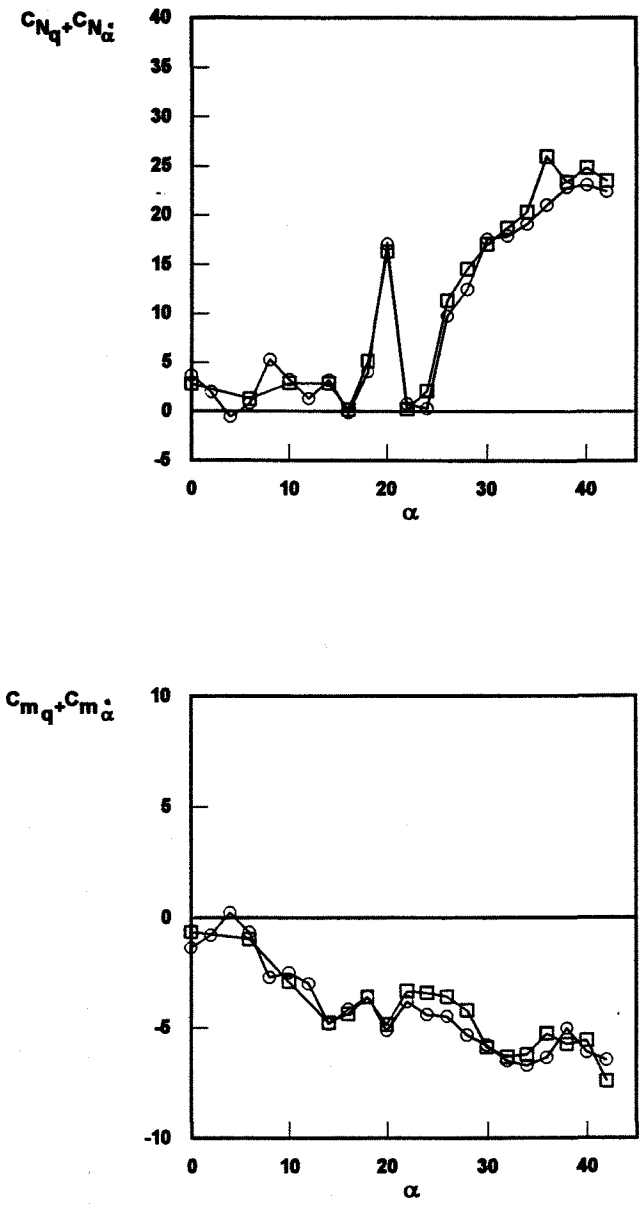

FIGURE 10 - Repeatability of dynamic data acquisition